

# Interplay between lattice-scale physics and the quantum Hall effect in graphene

Jason Alicea<sup>1</sup> and Matthew P. A. Fisher<sup>2</sup>

<sup>1</sup>Physics Department, University of California, Santa Barbara, CA 93106

<sup>2</sup>Microsoft Research, Station Q, University of California, Santa Barbara, CA 93106

(Dated: November 30, 2018)

Graphene's honeycomb lattice structure underlies much of the remarkable physics inherent in this material, most strikingly through the formation of two "flavors" of Dirac cones for each spin. In the quantum Hall regime, the resulting flavor degree of freedom leads to an interesting problem when a Landau level is partially occupied. Namely, while Zeeman splitting clearly favors polarizing spins along the field, precisely how the states for each flavor are occupied can become quite delicate. Here we focus on clean graphene sheets in the regime of quantum Hall ferromagnetism, and discuss how subtler lattice-scale physics, arising either from interactions or disorder, resolves this ambiguity to measurable consequence. Interestingly, such lattice-scale physics favors microscopic symmetry-breaking order coexisting with the usual liquid-like quantum Hall physics emerging on long length scales. The current experimental situation is briefly reviewed in light of our discussion.

PACS numbers: 73.43.-f, 71.10.-w, 71.10.Pm

## I. INTRODUCTION

Whereas electrons confined to 2D in conventional GaAs heterostructures are well-represented as residing in a continuous space, the behavior of electrons in graphene is inextricably tied to their underlying honeycomb lattice structure. This simple fact is central to much of the exceptional physics in the graphene quantum Hall effect. Most dramatically, in zero field the honeycomb band structure supports two Dirac cones centered at momenta  $\pm\mathbf{Q} = \pm(4\pi/3, 0)$ , so that graphene realizes a "relativistic" dispersion (over a significant energy range). In the presence of a perpendicular magnetic field, the Dirac spectrum develops into Landau levels that are approximately four-fold degenerate, one factor of two coming from spin and the other from the two "flavors" of Dirac cones. Taking into account this degeneracy as well as a Berry phase acquired from the cyclotron motion leads to the prediction of quantized Hall plateaus<sup>1,2,3,4</sup> with  $\sigma_{xy} = \nu e^2/h = 4(j + 1/2)e^2/h$ , whose observation was one of the early achievements in the study of graphene<sup>5,6</sup>.

The Landau level structure as well as the formation of these plateaus can be readily captured by a continuum Dirac equation with SU(4) symmetry (reflecting invariance under spin and flavor rotations), with no further considerations of graphene's lattice structure. In a sense, the problem then becomes rather similar to GaAs 2D electron systems, with a modified spectrum. But is this the full story? Simple symmetry considerations suggest that it is not. The approximate four-fold Landau level degeneracy noted above is clearly broken down by Zeeman coupling, but this still leaves an SU(2) flavor symmetry in the continuum theory. This residual symmetry can certainly be *spontaneously* broken, as occurs due to Coulomb exchange in quantum Hall ferromagnetism wherein plateaus occur at *all* integer filling factors (see the reviews of Refs. 7,8). However, it is important to observe that there is no microscopic reason for its existence in the first place. This suggests that *something* can, and will, *explicitly* lift this degeneracy further. Such effects were absent in initial experiments, due presumably to their being overshadowed by disorder. Given the observation of additional  $\nu = 0, \pm 1$ , and

$\pm 4$  plateaus at higher magnetic fields<sup>9,10</sup> as well as the inevitable future enhancement of sample quality, the question of precisely how the flavor degeneracy is lifted in graphene quantum Hall states is not only interesting, but also relevant. Such issues are important to resolve for a number of reasons. For instance, what is the precise nature of these new integer quantum Hall states? Looking forward, what type of states should be anticipated in the fractional regime? How do the low-lying excitations behave? What, if any, symmetries are broken in such states? And how can such properties be detected?

The central goal of this short review is to demonstrate that subtler lattice-scale physics provides such a degeneracy-lifting mechanism. There are a number of possible sources for this physics, which have been briefly summarized in Ref. 7. Here we will expand on some of these ideas, concentrating on clean graphene systems in the regime of quantum Hall ferromagnetism, which we believe to be of current experimental relevance. For the most part, we will examine a continuum Dirac theory derived from a simple lattice Hamiltonian that incorporates the electron kinetic energy and Coulomb repulsion, and demonstrate that such a minimal model indeed propagates important flavor-symmetry-breaking interactions into the continuum. Interestingly, this model predicts that quantum Hall states at filling factors  $\nu = \pm 1$  are not liquid-like at all on the lattice scale, but rather exhibit microscopic charge density wave order. Similarly, a broken-symmetry pattern with a tripled unit cell is favored at other odd-integer  $\nu$ . (See Fig. 2.) We then briefly summarize a recent numerical study of such an interacting lattice model<sup>11</sup>, which confirms these conclusions in the clean limit and extends the analysis by incorporating disorder. An alternate degeneracy-lifting mechanisms originating from disorder-driven variations in the electron hopping strengths as proposed by Abanin *et al.*<sup>12</sup> is also reviewed. Finally, we conclude with a brief assessment of the current experimental situation regarding these subtle yet interesting lattice-scale effects.

## II. CONTINUUM THEORY FROM AN INTERACTING LATTICE MODEL

A minimal lattice model for graphene that can be expected to realize integer and fractional quantum Hall states when a strong magnetic field is turned on should consist of two parts: electron kinetic energy plus Coulomb repulsion. It is reasonable, then, to start by understanding the physics contained in such a Hamiltonian, which we write using second quantization as

$$H = H_{\text{KE}} + H_{\text{Coul}}, \quad (1)$$

$$H_{\text{KE}} = -t \sum_{\langle \mathbf{x}\mathbf{x}' \rangle} \sum_{\alpha=\uparrow,\downarrow} [c_{\alpha\mathbf{x}}^\dagger c_{\alpha\mathbf{x}'} + \text{H.c.}], \quad (2)$$

$$H_{\text{Coul}} = U \sum_{\mathbf{x}} \left[ \frac{1}{4} (n_{\mathbf{x}})^2 - \frac{1}{3} \mathbf{S}(\mathbf{x})^2 \right] + \frac{1}{2} \sum_{\mathbf{x} \neq \mathbf{x}'} V(\mathbf{x} - \mathbf{x}') n_{\mathbf{x}} n_{\mathbf{x}'}. \quad (3)$$

In these expressions,  $c_{\alpha\mathbf{x}}^\dagger$  is the electron creation operator for spin  $\alpha$ ,  $n_{\alpha\mathbf{x}} = c_{\alpha\mathbf{x}}^\dagger c_{\alpha\mathbf{x}}$  is the corresponding electron number operator,  $n_{\mathbf{x}} = n_{\uparrow\mathbf{x}} + n_{\downarrow\mathbf{x}}$ , and  $\mathbf{S}(\mathbf{x}) = \frac{1}{2} c_{\alpha\mathbf{x}}^\dagger \boldsymbol{\sigma}_{\alpha\beta} c_{\beta\mathbf{x}}$  is the usual spin operator with  $\boldsymbol{\sigma}$  a vector of Pauli matrices. The first term in  $H_{\text{Coul}}$  contains the on-site repulsion energy, written in a manifestly SU(2)-invariant form, while the second represents the long-range part of the Coulomb repulsion, with  $V(\mathbf{x})$  the Coulomb potential. Normal ordering of the operators in Eq. (3) is understood.

The kinetic energy term in the Hamiltonian can be readily diagonalized to reveal two Dirac points at momenta  $\pm\mathbf{Q} = \pm(4\pi/3, 0)$ , which lie at the Fermi level when there is one electron per site. To describe excitations near the two nodes, it is highly convenient to pass to a continuum formulation by expanding the momentum-space fermion operators in terms of two flavors of continuum Dirac fermion fields (denoted  $R$  and  $L$ ) as follows,

$$c_{\alpha\mathbf{q}+\mathbf{Q}a} \sim \gamma \psi_{\alpha R a}(\mathbf{q}) \quad (4)$$

$$c_{\alpha\mathbf{q}-\mathbf{Q}a} \sim \gamma i \eta_{ab}^j \psi_{\alpha L b}(\mathbf{q}), \quad (5)$$

where  $\gamma = \sqrt{2}/(3^{1/4}l)$  ( $l$  is the linear system size). Here and below we reserve indices  $\alpha, \beta$  for spin,  $A, B$  for flavor, and  $a, b$  for the honeycomb sublattice. It is also useful to employ Pauli matrices  $\sigma_{\alpha\beta}^j$ ,  $\tau_{AB}^j$ , and  $\eta_{ab}^j$  that contract with the spin, flavor, and sublattice indices, respectively. We will use the convention that suppressed indices on the fields are implicitly summed (*i.e.*,  $\psi^\dagger \psi \equiv \sum_{\alpha A a} \psi_{\alpha A a}^\dagger \psi_{\alpha A a}$ ).

With these identifications, it is straightforward to recast the full interacting Hamiltonian into a continuum Dirac theory. Upon turning on the external magnetic field, one can essentially guess the leading kinetic energy and interaction terms, namely

$$\mathcal{H}_0 = -i\hbar v \int d^2\mathbf{x} \psi^\dagger [\eta^x D_x + \eta^y D_y] \psi + \frac{1}{2} \int d^2\mathbf{x} d^2\mathbf{x}' \rho_{\text{tot}}(\mathbf{x}) V(\mathbf{x} - \mathbf{x}') \rho_{\text{tot}}(\mathbf{x}'), \quad (6)$$

with  $v \approx 10^6$  m/s the Fermi velocity,  $D_j = \partial_j - i(e/\hbar)A_j$ , and  $\rho_{\text{tot}} = \psi^\dagger \psi$  the total density. For concreteness we take the magnetic field  $\mathbf{B} = \nabla \times \mathbf{A}$  in the  $+\hat{z}$  direction, normal to the graphene sheet. These contributions clearly exhibit an SU(4) symmetry, being invariant under arbitrary spin/flavor rotations. A more careful derivation, however, reveals a number of anisotropy terms, which break this SU(4) symmetry down to  $U(1)_{\text{spin}} \times [U(1) \times Z_2]_{\text{flavor}}$ . Writing the full Hamiltonian as  $\mathcal{H} = \mathcal{H}_0 + \mathcal{H}_1$ , these additional interactions can be written as follows,

$$\mathcal{H}_1 = \int d^2\mathbf{x} \left\{ -g\mu_B \mathbf{B} \cdot \mathbf{S}_{\text{tot}} + \frac{1}{4} u_0 [\rho_{\text{tot}}^2 + \rho_{\text{stag}}^2] - \frac{8}{3} (\mathbf{S}_{R1}^2 + \mathbf{S}_{L2}^2 + 6\mathbf{S}_{R1} \cdot \mathbf{S}_{L2} + (1 \leftrightarrow 2)) \right. \\ \left. - \sum_{\mathbf{r}} v_1(\mathbf{r}) \rho_{\text{stag}}(\mathbf{x} + \mathbf{r}) \rho_{\text{stag}}(\mathbf{x}) - u_2 [J_+^\dagger J_+ + J_-^\dagger J_-] \right\}, \quad (7)$$

where  $\mathbf{S}_{\text{tot}} = \frac{1}{2} \psi^\dagger \boldsymbol{\sigma} \psi$  is the uniform spin density,  $\rho_{\text{stag}} = \psi^\dagger \tau^z \eta^z \psi$  represents the staggered electron density between sublattices 1 and 2 of the honeycomb (see Fig. 2),  $\mathbf{S}_{Aa} = \frac{1}{2} \psi_{Aa}^\dagger \boldsymbol{\sigma} \psi_{Aa}$ , and  $J_+ = \psi_{R1}^\dagger \psi_{L2}$  and  $J_- = \psi_{R2}^\dagger \psi_{L1}$  represent components of the density oscillating at wave vectors  $\pm 2\mathbf{Q}$ . The sum in Eq. (7) is over Bravais lattice vectors. Once again, normal ordering is understood in the interactions above.

While the presence of these short-range anisotropy terms is not *a priori* obvious (apart from the Zeeman coupling), each has a simple physical interpretation. The second term in Eq. (7) merely encodes the on-site  $U$  repulsion; displaying the lattice constant  $a_0$  explicitly, we have

$$u_0 = \sqrt{3} a_0^2 U / 4. \quad (8)$$

The third, whose coupling is given by

$$v_1(\mathbf{r}) = \frac{\sqrt{3} a_0^2}{8} [V(\mathbf{r} + a_0/\sqrt{3} \hat{\mathbf{y}}) - (1 - \delta_{\mathbf{r},\mathbf{0}}) V(\mathbf{r})], \quad (9)$$

represents an inter-sublattice repulsion that reflects the smaller Coulomb energy cost for electrons residing on the same sublattice versus opposite sublattices. While this interaction is certainly short-ranged, the above non-local form must be retained when dealing with filling factors  $\nu = \pm 1$  to have an effect. At other integer filling factors, however, a purely local form suffices, and one can replace

$$\sum_{\mathbf{r}} v_1(\mathbf{r}) \rho_{\text{stag}}(\mathbf{x} + \mathbf{r}) \rho_{\text{stag}}(\mathbf{x}) \rightarrow u_1 \rho_{\text{stag}}^2, \quad (10)$$

$$u_1 \approx \frac{1}{\sqrt{3}} a_0^2 \left( \frac{e^2}{4\pi\epsilon a_0} \right), \quad (11)$$

where  $\epsilon$  is the (unscreened) dielectric constant. The final term represents the intra-sublattice repulsion between density components oscillating at  $\pm 2\mathbf{Q}$ , with

$$u_2 \approx \frac{4}{\sqrt{3}} u_1. \quad (12)$$

We note that the  $u_2$  interaction was also noticed by Goerbig *et al.*,<sup>13</sup> though at odd-integer filling factors we find that the  $v_1$  term provides the leading flavor-symmetry-breaking interaction.

Before turning to the implications of these interactions for quantum Hall states, it is useful to note the hierarchy of energy scales in the problem. The kinetic energy term in the SU(4)-invariant  $\mathcal{H}_0$  gives rise to four-fold degenerate Landau levels<sup>1,14</sup> indexed by an integer  $n$ , with energies  $E_n = \text{sign}(n)\sqrt{2e\hbar v^2 B|n|}$ . The spacing between the  $n = 0$  and  $n = \pm 1$  levels is the largest energy scale at roughly  $400\sqrt{B[\text{T}]}$  K, where  $B[\text{T}]$  is the magnetic field evaluated in Teslas. The characteristic Coulomb energy scales with the field in the same way:

$$\mathcal{E}_C \equiv \frac{e^2}{4\pi\epsilon_{\text{RPA}}\ell_B} \sim 100\sqrt{B[\text{T}]} \text{ K}, \quad (13)$$

where  $\ell_B$  is the magnetic length and  $\epsilon_{\text{RPA}}$  is the screened dielectric constant computed within the random phase approximation<sup>15</sup>, which yields  $\epsilon_{\text{RPA}} \approx 5\epsilon_0$ . The energies associated with the symmetry-breaking terms in  $\mathcal{H}_1$  are much smaller at laboratory fields. The Zeeman energy for instance is  $g\mu_B B \sim B[\text{T}]$  K. Furthermore, as emphasized in Ref. 13 the energies for the short-range interactions in  $\mathcal{H}_1$  are down by factors of  $a_0/\ell_B$  compared with  $\mathcal{E}_C$ . The associated scale for these terms is

$$\mathcal{E}_{\text{short-range}} \equiv \frac{e^2}{4\pi\epsilon a_0} \left(\frac{a_0}{\ell_B}\right)^2 \sim B[\text{T}] \text{ K}, \quad (14)$$

the first factor being the characteristic lattice-scale Coulomb energy and the second reflecting the average number of electrons in the highest occupied Landau level per unit cell. As we will discuss below, an exception occurs at filling factors  $\nu = \pm 1$ , where the scale for flavor symmetry breaking is down by an additional factor of  $a_0/\ell_B$ . Given the clear separation in energy scales above, it is reasonable to first consider the physics contained in  $\mathcal{H}_0$ , and then take into account the additional symmetry-breaking terms in  $\mathcal{H}_1$ . This is the strategy we will follow below.

### III. IMPLICATIONS FOR QUANTUM HALL STATES

Let us now very briefly review some aspects of integer quantum Hall physics expected from the SU(4) invariant Hamiltonian  $\mathcal{H}_0$ . Apart from the integer quantum Hall states occurring at filling factors  $\nu = 4(j + 1/2)$ , where the highest occupied Landau level is completely full, it is well-established that quantum Hall ferromagnetism emerges at other integer filling factors due to Coulomb exchange<sup>7,8,16</sup>. Here, in the absence of anisotropy terms the SU(4) symmetry enjoyed by  $\mathcal{H}_0$  is broken spontaneously, giving way to gapless Goldstone modes analogous to spin waves<sup>17</sup> (the number depends on  $\nu$ ) and SU(4) skyrmions<sup>18,19</sup> that provide the lowest-energy charge excitations in the  $n = 0, \dots, \pm 3$  levels<sup>17</sup>.

The physics of quantum Hall ferromagnetism in graphene is substantially modified by the anisotropy terms in  $\mathcal{H}_1$ . Only

a subset of the SU(4) symmetry will be spontaneously broken, the Goldstone modes will generally become gapped, and the skyrmion character will change as well. Here we will focus for the most part on elucidating the qualitative features of these effects, obtained within a Hartree-Fock framework; quantitative aspects have been discussed elsewhere<sup>17,20,21</sup>. We will specialize to the  $n = 0$  and  $n = 1$  Landau levels ( $n = -1$  is related by particle-hole symmetry). To this end, we first note a simple yet crucial feature of the Landau level wave functions that will prove illuminating. Namely, the  $n = 0$  single-particle wave functions for flavor  $L$  reside entirely on honeycomb sublattice 1, while flavor  $R$  states reside entirely on sublattice 2. In contrast, the probability weight for  $n \neq 0$  wave functions is evenly distributed between both sublattices. The effect of  $\mathcal{H}_1$  in these two cases differs completely as a result of this distinction.

Consider the  $n = 0$  Landau level first. Employing the standard Landau level projection, the interactions simplify greatly here due to the character of the wave functions noted above, with the  $u_2$  term dropping out entirely. At filling factor  $\nu = -1$ , corresponding to a quarter-filled level, Zeeman coupling clearly favors a spin-polarized state; the on-site  $U$  interaction can then play no role due to Pauli exclusion. The fate of the flavor degree of freedom is thus set by the sublattice repulsion in  $\mathcal{H}_1$ . It is useful to note that a general flavor-polarized state can be expressed as

$$|\theta, \phi\rangle = \prod_{m=0}^{\infty} \left[ \cos \frac{\theta}{2} c_{\uparrow R, m}^\dagger + \sin \frac{\theta}{2} e^{i\phi} c_{\uparrow L, m}^\dagger \right] |\text{vac}\rangle, \quad (15)$$

where  $c_{\uparrow A, m}^\dagger$  adds a spin-up, flavor- $A$  particle with angular momentum  $m$  into the  $n = 0$  Landau level and  $|\text{vac}\rangle$  corresponds to the empty  $n = 0$  level. The angles  $\theta, \phi$  specify the polarization direction in “flavor space”, shown schematically in Fig. 1. In particular, “easy-axis” flavor polarization is favored here, with  $\theta = 0$  or  $\pi$ , resulting in a state with all the electrons occupying the  $n = 0$  level spontaneously choosing to reside on one honeycomb lattice as shown in Fig. 2(a). The physics behind this microscopic charge density wave (CDW) is simple: the electrons can stay farther apart from one another by remaining on one sublattice.

It is important to note that this effect is rather weak. First, the gap  $\Delta_f$  for exciting “flavor waves” (which weakly modulate the system away from the perfect CDW, much like a spin wave) is quite small:

$$\Delta_f \approx 4 \times 10^{-3} (B[\text{T}])^{3/2} \text{ K}, \quad (16)$$

which is down by an extra small factor of  $a_0/\ell_B$  compared to  $\mathcal{E}_{\text{short-range}}$  in Eq. (14). Despite appearances, a local  $\rho_{\text{stag}}^2$  interaction is insensitive to  $\theta$  and  $\phi$  above, for the same reason that  $(S^z)^2$  is trivial for a spin-1/2 moment. Rather, it is the non-local part of the sublattice repulsion in  $\mathcal{H}_1$  that provides the degeneracy lifting, resulting in the additional small factor noted above. The spin-wave gap, by contrast, is much larger at  $\Delta_s = g\mu_B B \approx B[\text{T}]$  K; hybrid “spin-flavor waves” cost a similar energy. The smallness of the flavor anisotropy implies that “flavor skyrmions” will provide the lowest-energy

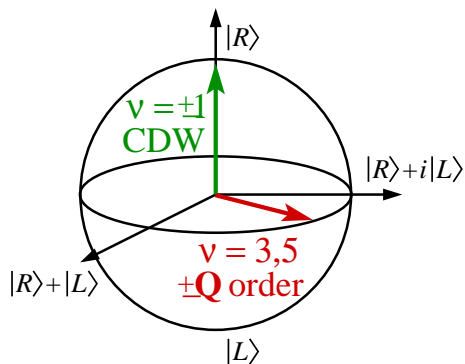


FIG. 1: Order-parameter space for flavor-polarized states. Interactions favor “easy-axis” polarization at  $\nu = \pm 1$ , but “easy-plane” polarization at  $\nu = 3, 5$ . The corresponding lattice-scale order is shown schematically in Fig. 2. Disorder of the type discussed in Sec. V, however, favors easy-plane polarization at  $\nu = \pm 1$ .

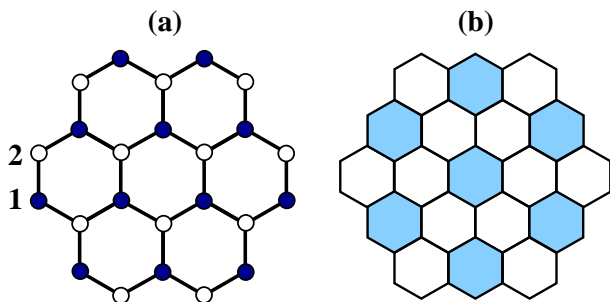


FIG. 2: Lattice-scale symmetry-breaking patterns favored by interactions at (a)  $\nu = \pm 1$  and (b)  $\nu = 3, 5$ . On the left, the electron density is higher on one of the two sublattices. On the right translation symmetry is broken, along with, in general, rotation and reflection symmetries due to the formation of lattice-scale currents circulating around hexagons. For example, one such ordering involves currents circulating uniformly around the shaded hexagons.

charge excitations, but also suggests that other mechanisms not included here may influence the flavor degree of freedom, as we will discuss below. Second, only the relatively small number of electrons in the  $n = 0$  level participate in the CDW (around  $1.4 \times 10^{-5} B[\text{T}]$  electrons per hexagon), though in principle its presence may be detected with STM or NMR measurements<sup>20</sup>. Analogous results hold for the particle-hole related  $\nu = 1$  filling factor.

The ground state at  $\nu = 0$  depends on the competition between Zeeman coupling and the on-site  $U$  versus the sublattice repulsion, which is much more effective here since even a local  $\rho_{\text{stag}}^2$  interaction behaves nontrivially on polarized states. If the former dominate, then the ground state will clearly be spin-polarized, with electrons equally occupying both sublattices. This transpires provided  $g\mu_B B + 2u_0\rho_0 > 4u_1\rho_0$ , where  $\rho_0 = 1/(2\pi\ell_B^2)$  is the density of a quarter-filled Landau level. For clean graphene sheets on a  $\text{SiO}_2$  substrate, we estimate that this inequality is satisfied if  $U \gtrsim 4$  eV. Otherwise the sublattice repulsion will dominate, and a spin-singlet

CDW emerges. We emphasize that here the CDW order can be much more robust than at  $\nu = \pm 1$ , the flavor-wave gap now being set by  $4u_1\rho_0 - (g\mu_B B + 2u_0\rho_0)$  which should generically be of order  $\mathcal{E}_{\text{short-range}}$ . Which scenario prevails is unclear because of uncertainties in the magnitude of  $U$ ,<sup>22</sup> though a spin-polarized state can always be achieved by tilting the field to enhance the effective  $g$ -factor. In either case, the charge gap is expected to be set by mixed spin/flavor-textured skyrmions. For instance, in the spin-polarized state skyrmions will have lower energy if they degrade the spin polarization while simultaneously restoring CDW order. The dependence of the activation energy on an in-plane field can allow one to distinguish between these ground states. An increase is expected in the spin-polarized state since the larger effective  $g$ -factor reduces the optimal skyrmion size and hence raises their energy, while a decrease is expected for the spin-singlet CDW since here skyrmions induce a revival of spin polarization.

Next we discuss the  $n = 1$  Landau level, beginning with filling factor  $\nu = 3$ . The physics is similar for  $\nu = 5$  and will not be discussed separately. Since the wave functions now live equally on both sublattices, one must wrestle with all terms in  $\mathcal{H}_1$ . Satisfying the Zeeman coupling requires full spin polarization, so again the on-site  $U$  repulsion drops out. A general flavor-polarized state can be written as in Eq. (15), with the creation operators now filling  $n = 1$  Landau levels. Both the  $u_1$  and  $u_2$  terms lift the ordering degeneracy here, though the effects are subtle since the form of the wave functions dictates that  $\langle \rho_{\text{stag}} \rangle = \langle J_{\pm} \rangle = 0$  for any  $\theta, \phi$ . Rather, the symmetry-breaking comes from exchange contributions. In particular,  $u_1$  favors “easy-plane” polarization, *i.e.*,  $\theta = \pi/2$  and arbitrary  $\phi$ , while  $u_2$  favors easy-axis polarization. A quantitative estimate suggests that the former easy-plane state, which is characterized by an order parameter  $\langle \psi^\dagger (\tau^x + i\tau^y) \psi \rangle \neq 0$ , has lower energy. This state is ordered at wave vectors  $\pm \mathbf{Q}$ , and exhibits the symmetry-breaking pattern shown in Fig. 2(b). In general, rotation and reflection symmetries are broken as well, due to the formation of lattice-scale currents circulating around honeycomb plaquettes. The specific pattern of currents is determined by  $\phi$ , which within our theory is selected spontaneously. Consequently, one would expect a finite-temperature Kosterlitz-Thouless transition, which has yet to be definitively observed in a quantum Hall system. While graphene may eventually provide a clean setting for realizing this physics, we note that (presumably) higher-order lattice effects will energetically favor specific values of  $\phi$ .

At filling factor  $\nu = 4$ , the ground state depends on the strength of Zeeman coupling and the on-site  $U$  relative to the  $u_1$  and  $u_2$  interactions. The former terms favor a fully spin-polarized state, while the latter favor a spin-singlet state with easy-plane flavor polarization. Variational energetics suggest that for reasonable values of  $U$  the ground state is spin polarized, and hence does not exhibit lattice-scale order.

Similar physics can be expected at higher- $|n|$  Landau levels, although this problem has not yet been examined quantitatively. With regard to fractional quantum Hall states, which have been studied theoretically<sup>3,17,23,24,25,26</sup> but not yet observed, the anisotropy terms considered here should be kept

in mind, particularly in situations where a number of states are energetically competitive.

#### IV. NUMERICS

The picture presented above for the nature of quantum Hall states at odd-integer filling factors is supported by recent numerics by Sheng *et al.*<sup>11</sup> These authors carried out an exact diagonalization study of the interacting Hamiltonian in Eq. (1), incorporating the magnetic field directly on the lattice (*i.e.*, sending  $t \rightarrow te^{iA_{\mathbf{x}\mathbf{x}'}}$ , where  $A_{\mathbf{x}\mathbf{x}'}$  is the lattice vector potential, and including the Zeeman energy) and additionally allowing for random on-site chemical potential disorder. Assuming the Zeeman splitting is sufficiently large so that spin-up and spin-down Landau levels are well-separated, the many-body wave functions were obtained exactly upon projecting onto the highest occupied Landau level. Up to 24 electrons in the projected level were considered, in systems with linear dimensions up to  $200 \times 200$  and periodic boundary conditions.

In the clean limit appropriate to the discussion above, spin- and flavor-polarized ground states are found numerically at filling factors  $\nu = -1$  and  $\nu = 3$ . In particular, a clear easy-axis anisotropy is observed at  $\nu = -1$ , corresponding to the lattice-scale CDW order of Fig. 2(a). The anisotropy energy characterizing the energy difference between the easy-axis and easy-plane polarized states (see Fig. 1) is indeed found to be quite small, on the order of  $\mathcal{E}_C(a_0/\ell_B)^2$  as expected from our Hartree-Fock analysis. Again, we note that this is down by a factor of  $a_0/\ell_B$  compared to  $\mathcal{E}_{\text{short-range}}$  since a local  $\rho_{\text{stag}}^2$  interaction does not split the ordering degeneracy. Unfortunately, the smallness of the anisotropy energy did not permit numerical resolution of the correspondingly small gap  $\Delta_f$  for flavor-waves out of the easy-axis state. At  $\nu = 3$ , easy-plane flavor polarization emerges. A strong finite-size effect supports the lattice-scale structure predicted for this state [see Fig. 2(b)]. Specifically, the easy-plane state occurs only if both linear dimensions of the system are divisible by 3; otherwise easy-axis polarization occurs, since the ordering at wave vectors  $\pm\mathbf{Q}$  would then be “frustrated” at the boundaries. Finite-size scaling suggests that the easy-plane state wins in the thermodynamic limit, since the ground-state energy per particle exhibits an upturn when the easy-axis state occurs. Thus, numerics are entirely consistent with our analytic predictions for the clean limit, and, importantly, can provide valuable information about the stability of quantum Hall ferromagnetism when disorder is included, as we will mention briefly at the end of this review.

#### V. DISORDER EFFECTS AT $\nu = \pm 1$

We now return to filling factors  $\nu = \pm 1$ , where the flavor symmetry breaking encoded in the interacting lattice model we have been focusing on was found to be rather weak. Abanin *et al.*<sup>12</sup> have proposed an interesting alternative effect which may provide the dominant flavor symmetry breaking mechanism—*disorder*. Real graphene sheets inevitably

exhibit some degree of structural imperfection, which may arise for instance from the presence of a substrate. Atomic force microscopy on graphene samples examined in Ref. 27 revealed surface ripples with a typical lateral length  $\xi$  of a few tens of nanometers (though ensuing fabrication advances produced higher-mobility samples with ripples below the resolution of their microscope<sup>27</sup>). Such distortions give rise to spatially varying electron hopping strengths, which appear as an effective inhomogeneous magnetic field in the continuum, directed oppositely for the two flavors. In our notation this corresponds to sending

$$D_j \rightarrow D_j - i(e/\hbar)a_j(\mathbf{x})\tau^z \quad (17)$$

in Eq. (6), where  $\vec{\delta h}(\mathbf{x}) = \nabla \times \mathbf{a}$  is the effective field, whose magnitude was estimated to be around 0.1 to 1 T in Ref. 27. The vector potential  $\mathbf{a}$ , being proportional to the local hopping strength deviations, was assumed to have white noise correlations with a correlation length  $\xi$  in Ref. 12.

One possible consequence of this random field is that the system may break up into domains with local easy-axis flavor polarization (*i.e.*, local CDW order) specified by the direction of  $\vec{\delta h}$ , at the cost of domain wall energy. This is the Larkin-Imry-Ma state<sup>28,29</sup>. Abanin *et al.*, however, argue that an easy-plane flavor-polarized state is energetically more favorable, at least for weak disorder. The physics behind this easy-plane selection can be understood by analogy to a ferromagnet, where spins preferentially align *perpendicular* to an applied field so they they can effectively gain energy by relaxing toward it. Just as we discussed at  $\nu = 3$  and 5, the easy-plane state here will exhibit a Kosterlitz-Thouless transition; the transition temperature was estimated to be a few Kelvin in Ref. 12. The easy-plane anisotropy arising from disorder was estimated to be

$$\Delta_{\text{disorder}} \sim \left(\frac{\delta h}{B}\right)^2 \left(\frac{\xi}{\ell_B}\right)^2 \mathcal{E}_C \sim \frac{(\delta h[\text{T}]\xi[\text{nm}])^2}{10\sqrt{B[\text{T}]}} \text{K}, \quad (18)$$

where  $\delta h[\text{T}]$  is the typical effective field strength in Teslas and  $\xi[\text{nm}]$  is the disorder correlation length in nanometers. With  $\delta h$  in the range of 0.1 to 1 T and  $\xi \sim 30$  nm, this may indeed significantly exceed the intrinsic anisotropy  $\Delta_f$  arising from interactions. For systems with less structural imperfection<sup>27</sup>, however, the competition between disorder and interactions may be quite delicate.

#### VI. CONCLUDING REMARKS

We conclude by discussing the current experimental situation regarding the physics of quantum Hall ferromagnetism in graphene. Although  $\nu = \pm 4$  plateaus have been observed at high magnetic fields ( $B \gtrsim 20$  T),<sup>9,10</sup> quantum Hall ferromagnetism is apparently not yet realized in the  $n = 1$  Landau level. Plateaus at  $\nu = 3, 5$  have yet to be resolved, and the activation energy at  $\nu = 4$  was found to be dominated by Zeeman splitting of the spin-up and spin-down states, rather than Coulomb energy as would be expected for a clean system. The situation is entirely different for the  $n = 0$  Landau

level, where  $\nu = 0$  and  $\pm 1$  quantum Hall states have all been observed<sup>9,10</sup>. Furthermore, the activation energy measured at  $\nu = 1$  was several times larger than that at  $\nu = \pm 4$  and found to scale with  $\sqrt{B}$ , suggesting Coulomb exchange as the origin of the gap<sup>10</sup>. Thus current experimental graphene samples appear sufficiently clean to enable observation of quantum Hall ferromagnetism in the  $n = 0$  level, but not at other levels. It is worth emphasizing that the greater stability of ferromagnetism to disorder in the  $n = 0$  level is fully consistent with theory. Nomura and MacDonald derived a Stoner criterion for the onset of interaction-driven quantum Hall states, which predicts a critical mobility for spontaneous symmetry breaking that is several times larger in the  $n = 1$  level than in the  $n = 0$  level<sup>16</sup>. More recently, the numerical study by Sheng *et al.*<sup>11</sup> finds a critical on-site disorder strength for observing a plateau at  $\nu = 3$  to be roughly one third that at  $\nu = 1$ .

Resolving the more detailed symmetry-breaking order inherent in the likely exchange-driven  $\nu = 0$  and  $\pm 1$  quantum Hall states remains an open experimental challenge. Ultimately, local probes such as STM and NMR measurements

would be ideal for detecting possible microscopic patterns such as those in Fig. 2, though such experiments may be difficult since the order would involve only a small fraction of the total number of electrons. Such symmetry breaking may also be revealed by possible concomitant lattice distortions. On a cruder level, the qualitative trend in the activation energy as a function of field might provide some clues as to the nature and origin of these states. At  $\nu = \pm 1$  for instance, the intrinsic anisotropy due to interactions scales as  $B^{3/2}$ , while the anisotropy due to disorder predicted by Abanin *et al.* scales as  $B^{-1/2}$ . Consequently, the energy for skyrmions relative to those in the SU(4)-symmetric case should increase with field in the former case, but decrease in the latter, which may be revealed through measurements of the activation energy.

*Acknowledgments.* — We would like to thank Leon Balents, Allan MacDonald, Kun Yang, and Philip Kim for stimulating discussions. This work was supported by the National Science Foundation through grants PHY-9907949 (M. P. A. F.) and DMR-0210790 (J. A. and M. P. A. F.).

- 
- <sup>1</sup> Y. Zheng and T. Ando, Phys. Rev. B **65**, 245420 (2002).  
<sup>2</sup> V. P. Gusynin and S. G. Sharapov, Phys. Rev. Lett. **95**, 146801 (2005).  
<sup>3</sup> N. M. R. Peres, F. Guinea, and A. H. Castro Neto, Phys. Rev. B **73**, 125411 (2006).  
<sup>4</sup> A. H. Castro Neto, F. Guinea, and N. M. R. Peres, Phys. Rev. B **73**, 205408 (2006).  
<sup>5</sup> K. S. Novoselov, A. K. Geim, S. V. Morozov, D. Jiang, M. I. Katsnelson, I. V. Grigorieva, S. V. Dubonos, and A. A. Firsov, Nature **438**, 197 (2005).  
<sup>6</sup> Y. Zhang, Y.-W. Tan, H. L. Stormer, and P. Kim, Nature **438**, 201 (2005).  
<sup>7</sup> K. Yang, Solid State Communications **143**, 27 (2007).  
<sup>8</sup> S. M. Girvin, *The Quantum Hall Effect: Novel Excitations and Broken Symmetries*, in Les Houches Summer School 1998 (Springer Verlag and Les Editions de Physique, Paris, 1999).  
<sup>9</sup> Y. Zhang, Z. Jiang, J. P. Small, M. S. Purewal, Y.-W. Tan, M. Fazlollahi, J. D. Chudow, J. A. Jaszczak, H. L. Stormer, and P. Kim, Phys. Rev. Lett. **96**, 136806 (2006).  
<sup>10</sup> Z. Jiang, Y. Zhang, H. Stormer, and P. Kim, arXiv:0705.1102 (unpublished).  
<sup>11</sup> L. Sheng, D. N. Sheng, F. D. M. Haldane, and L. Balents, arXiv:0706.0371 (unpublished).  
<sup>12</sup> D. A. Abanin, P. A. Lee, and L. S. Levitov, Phys. Rev. Lett. **98**, 156801 (2007).  
<sup>13</sup> M. O. Goerbig, R. Moessner, and B. Douçot, Phys. Rev. B **74**, 161407 (2006).  
<sup>14</sup> F. D. M. Haldane, Phys. Rev. Lett. **61**, 2015 (1988).  
<sup>15</sup> J. Gonzalez, F. Guinea, and M. A. H. Vozmediano, Phys. Rev. B **59**, R2474 (1999).  
<sup>16</sup> K. Nomura and A. H. MacDonald, Phys. Rev. Lett. **96**, 256602 (2006).  
<sup>17</sup> K. Yang, S. D. Sarma, and A. H. MacDonald, Phys. Rev. B **74**, 075423 (2006).  
<sup>18</sup> S. L. Sondhi, A. Karlhede, S. A. Kivelson, and E. H. Rezayi, Phys. Rev. B **47**, 16419 (1993).  
<sup>19</sup> D. P. Arovas, A. Karlhede, and D. Lilliehook, Phys. Rev. B **59**, 13147 (1999).  
<sup>20</sup> J. Alicea and M. P. A. Fisher, Phys. Rev. B **74**, 075422 (2006).  
<sup>21</sup> R. L. Doretto and C. M. Smith, arXiv:0704.3671 (unpublished).  
<sup>22</sup> S. Chakravarty, S. Khlebnikov, and S. Kivelson, Phys. Rev. Lett. **69**, 212 (1992).  
<sup>23</sup> C. Toke, P. E. Lammert, J. K. Jain, and V. H. Crespi, Phys. Rev. B **74**, 235417 (2006).  
<sup>24</sup> V. M. Apalkov and T. Chakraborty, Phys. Rev. Lett. **97**, 126801 (2006).  
<sup>25</sup> C. Toke and J. K. Jain, arXiv:cond-mat/0701026 (unpublished).  
<sup>26</sup> M. O. Goerbig and N. Regnault, Phys. Rev. B **75**, 241405 (2007).  
<sup>27</sup> S. V. Morozov, K. S. Novoselov, M. I. Katsnelson, F. Schedin, L. A. Ponomarenko, D. Jiang, and A. K. Geim, Phys. Rev. Lett. **97**, 016801 (2006).  
<sup>28</sup> A. I. Larkin, JETP **31**, 784 (1970).  
<sup>29</sup> Y. Imry and S. K. Ma, Phys. Rev. Lett. **35**, 1399 (1975).